horticulturae

MDPI

Article

Using Optimized Three-Band Spectral Indices and a Machine Learning Model to Assess Squash Characteristics under Moisture and Potassium Deficiency Stress

Mohamed A. Sharaf-Eldin [1], Salah Elsayed [2,*], Adel H. Elmetwalli [3,*], Zaher Mundher Yaseen [4,5], Farahat S. Moghanm [6], Mohssen Elbagory [7,8,*], Sahar El-Nahrawy [8], Alaa El-Dein Omara [8], Andrew N. Tyler [9] and Osama Elsherbiny [10]

1 Horticulture Department, Faculty of Agriculture, Kafrelsheikh University, Kafr El-Sheikh 33516, Egypt
2 Agricultural Engineering, Evaluation of Natural Resources Department, Environmental Studies and Research Institute, University of Sadat City, Minufiya 32897, Egypt
3 Department of Agricultural Engineering, Faculty of Agriculture, Tanta University, Tanta 31527, Egypt
4 Civil and Environmental Engineering Department, King Fahd University of Petroleum and Minerals, Dhahran 31261, Saudi Arabia
5 Interdisciplinary Research Center for Membranes and Water Security, King Fahd University of Petroleum & Minerals, Dhahran 31261, Saudi Arabia
6 Soil and Water Department, Faculty of Agriculture, Kafrelsheikh University, Kafr El-Sheikh 33516, Egypt
7 Department of Biology, Faculty of Science and Arts, King Khalid University, Mohail 61321, Assir, Saudi Arabia
8 Agricultural Research Center, Department of Microbiology, Soils, Water and Environment, Research Institute, Giza 12112, Egypt
9 School of Biological and Environmental Sciences, University of Stirling, Stirling, Scotland FK9 4LA, UK
10 Agricultural Engineering Department, Faculty of Agriculture, Mansoura University, Mansoura 35516, Egypt
* Correspondence: salah.emam@esri.usc.edu.eg (S.E.); adel.elmetwali@agr.tanta.edu.eg (A.H.E.); mhmohammad@kku.edu.sa (M.E.)

Citation: Sharaf-Eldin, M.A.; Elsayed, S.; Elmetwalli, A.H.; Yaseen, Z.M.; Moghanm, F.S.; Elbagory, M.; El-Nahrawy, S.; Omara, A.E.-D.; Tyler, A.N.; Elsherbiny, O. Using Optimized Three-Band Spectral Indices and a Machine Learning Model to Assess Squash Characteristics under Moisture and Potassium Deficiency Stress. *Horticulturae* **2023**, *9*, 79. https://doi.org/10.3390/horticulturae9010079

Academic Editors: Alessia Cogato, Marco Sozzi and Eve Laroche-Pinel

Received: 12 November 2022
Revised: 23 December 2022
Accepted: 3 January 2023
Published: 7 January 2023

Abstract: Moisture and potassium deficiency are two of the main limiting variables for squash crop performance in many water-stressed places worldwide. If major output decreases are to be avoided, it is critical to detect signs of crop stress as early as possible in the growth cycle. Proximal remote sensing can be a reliable technique for offering a rapid and precise instrument and localized management tool. This study tested the ability of proximal hyperspectral remotely sensed data to predict squash traits in two successive seasons (spring and fall) with varying moisture and potassium rates. Spectral data were collected from drip-irrigated squash that had been treated to varied rates of irrigation and potassium fertilization over both investigated seasons. To forecast potassium-use efficiency (KUE), chlorophyll meter (Chlm), water-use efficiency (WUE), and seed yield (SY) of squash, different commonly used and newly-introduced spectral index values for three bands (3D-SRIs), as well as a Decision Tree (DT) model, were evaluated. The results revealed that the newly constructed three-band SRIs based on the wavelengths of the visible (VIS), near-infrared (NIR), and red-edge regions were sensitive enough to measure the four tested parameters of squash in this study. For instance, $NDI_{558,646,708}$ presented the highest R^2 of 0.75 for KUE, $NDI_{744,746,738}$ presented the highest R^2 of 0.65 for Chlm, and $NDI_{670,628,392}$ presented the highest R^2 of 0.64 for SY of squash. The results further demonstrated that the principal component analysis (PCA) demonstrated the ability to distinguish moisture stress from potassium deficiency stress at the flowering stage onwards. Combining 3D-SRIs, DT-based bands (DT-b), and the aggregate of all spectral characteristics (ASF) with DT models would be an effective strategy for estimating four observed parameters with appropriate accuracy. For example, the model's approximately 30 spectral characteristics were extremely important for predicting KUE. Its outputs with R^2 were, for the training and validation datasets, 0.967 (RMSE = 0.175) and 0.818 (RMSE = 0.284), respectively. For measuring Chlm, the DT-DT-b-20 model demonstrated the best. In the training and validation datasets, the R^2 value was 0.993 (RMSE = 0.522) and 0.692 (RMSE = 2.321), respectively. The overall outcomes showed that proximal-reflectance-sensing-based 3D-SRIs and DT models based on 3D-SRIs, DT-b, and ASF could be used to evaluate the four tested parameters of squash under different levels of irrigation regimes and potassium fertilizer.

Keywords: abiotic stress; *Cucurbita pepo*; potassium-use efficiency; water-use efficiency; seed yield

1. Introduction

Squash (*Cucurbita pepo* L.) is a popular cucurbit vegetable crop in many parts of the world. It is a commercial crop that is grown in both open fields and greenhouses, particularly in the Mediterranean region [1–3]. It provides numerous medicinal and health benefits for humans [4], as well as adequate levels of proteins, minerals, vitamins and carbohydrates for human nutrition [5].

Water scarcity is regarded as the most significant constraint to plant growth and development in arid and semi-arid environments, yielding more than any other environmental factors [6–10]. It is clear that a lack of water, even for a short period, alters the physio-biochemical characteristics of crops, which inhibits their growth and productivity [11–13].

Fertilization is also important for absorbing macronutrients, determining their amount in various plant organs, and determining final yield. Due to the quick accumulation of vegetable mass in a relatively short period of harvest, squash crops are fertilization-responsive vegetable crops [14–16]. Potassium is a vital nutrient for plant growth and development, so developing an optimal water–potassium fertilization management strategy to improve their application efficiency is crucial [17,18].

In locations where there is a lack of moisture and fertilization, agricultural crop production is always monitored using point-sampling techniques (traditional methods), which are laborious, expensive, and seem to have poor spatial representation [19–23]. Therefore, to support current agricultural practices, especially in nations where current agricultural systems are unable to meet the high demands of rapid population growth, robust and fast techniques for spotting stress in various agricultural crops are necessary. Accurate, rapid, non-destructive, and cost-effective estimation of a wide range of phenotypic crop traits is possible with the help of proximal remote sensing, which can complement or even replace traditional methods [24–26]. The remote sensing technique can detect even minor changes in various biophysical and biochemical aspects of the plant canopy caused by moisture and or fertilization deficiencies in the range from the visible (VIS) to the near-infrared (NIR) and shortwave infrared (SWIR). Broadly, changes in above-ground biomass, leaf pigments, leaf area index, leaf water content and nutrient content are reflected in changes in the crop canopy's spectral signature [27,28]. Plant pigments, such as chlorophyll and carotenoids, absorb a lot of visible light, especially blue and red light. Furthermore, the diffusion and scattering of radiation as a result of dry matter and leaf tissues has a significant impact on canopy reflectance in the NIR range [29–33].

Spectral vegetation indices derived from in situ ground-based remotely sensed data have been shown in prior studies to be useful for identifying stressed vegetation in a wide range of agricultural crops. These include, for example: the determination of aerial plant biomass [34–37]; chlorophyll a concentration [38–42]; crop grain yield [43,44]; leaf area index [45–47]; nitrogen content [48,49]; water stress [31,50]; pest injuries; and plant diseases [25,51,52]. Many earlier research studies have shown that ground-based remotely sensed data can be utilized to evaluate growth parameters and crop health status; however, most of the studies concentrated on detecting moisture shortage stress, whereas potassium deficiency has received comparatively less attention in the literature. This study examined the feasibility of utilizing ground-based remote sensing to detect potassium and moisture stress at the canopy scale. It is crucial to make measurements at the canopy scale in order to evaluate how well satellite imagery might be used for site-specific management.

Model-based feature selection methods, for example, identify a subset of features with strong discriminative and foretelling power [53]. By reducing extraneous features and limiting over-fitting, this method can improve model performance. Moreover, it retains the initial feature representation, which boosts interpretability [54]. Prediction and modeling increasingly require feature selection algorithms [55]. Many research studies have been conducted to investigate the use of various strategies for dimensionality reduction in data. Each variable's weighed regression coefficient in the partial least-squares (PLS) model highlights the importance of wavelength in the model for partial least-square regression (PLSR) [56]. In the decision tree (DT) and random forest (RF), all variables are ranked in order of relevance [57]. Glorfeld [58] created a back-propagation neural network index for identifying the most important variables. Furthermore, hyper-parameter selection has a substantial influence on the ability of any machine learning (ML) model, which has numerous benefits: it has the potential to improve the performance of ML algorithms [59], as well as the repeatability and fairness of scientific studies [60]. It might play a crucial role in improving the prediction model because it has direct influence over training algorithm behavior [61]. Consequently, we may expect that changing hyper-parameters will have a remarkable influence on the accuracy of squash crop quality measurements.

The objectives of the current study were to (i) estimate the effects of irrigation treatments and potassium fertilization on four traits of squash (KUE, Chlm, WUE and SY); (ii) evaluate the performance of common and three-band SRIs to assess the four traits of squash; (iii) assess the potential role of ground-based remote sensing based on spectral bands to detect and distinguish water and potassium stress spectrally; and (iv) evaluate the performance of the DT model based on the spectral bands, SRIs and data fusion of both spectral bands, and of SRIs to predict the four investigated traits of squash.

2. Materials and Methods

2.1. Experimental Description

Over the spring and fall seasons of 2018, two field experiments were conducted at a private farm in the Elshagaa region, Egypt (latitude of 30°4′12″ N and longitude of 30°19′48″ E). Non-disturbed soil samples were taken at two depths of the soil profile (0–30, and 30–60 cm) to identify some physical and chemical characteristics of the experimental soil, which was classified as loamy sand in texture, with an average bulk density of 1.53 g cm^{-3}, an electrical conductivity (EC) of 1.32 dS m^{-1}, and a pH of 7.39. The particle size distribution was found to be 87.3% sand, 6.36% silt, and 6.34% clay. The chemical analysis of the experimental soil, which includes cations and anions, is shown in Table 1. Squash was planted in the first week of March and the last week of July, with a growing season of around 100 days from planting to harvest. In addition, the soil's hydrophysical characteristics were determined as detailed in Table 2. Nitrogen fertilization in the form of ammonium nitrate was applied in three equal doses at 30, 45 and 60 days after planting at a rate of 285 kg N ha^{-1}.

Table 1. Some chemical analysis of the experimental soil at different depths.

Soil Depth, cm	EC, dS/m^{-1}	pH	Cations, Meq/L				Anions, Meq/L			
			Mg^{++}	Ca^{++}	K^{+}	Na^{+}	Co_3^{---}	HCo_3^{--}	Cl^{-}	So_4^{--}
0–30	1.32	7.39	3.2	3.21	1.28	4.77	0.0	2.71	7.18	2.54
30–60	1.17	7.21	3.33	3.34	1.37	4.61	0.0	2.77	7.36	2.51

Table 2. Mechanical analysis and some soil physical properties.

Depth, cm	ρ_b, g cm^{-3}	FC, %	WP, %	AW, %	Particle Size Distribution, %			Texture
					Sand	Silt	Clay	
0–30	1.40	16.9	9.34	7.56	87.3	6.36	6.34	Loamy sand
30–60	1.56	15.13	8.35	6.78	86.3	7.52	6.18	Loamy sand

FC, field capacity; WP, wilting point; AW, available water; ρ_b, bulk density.

2.2. Solar–Powered Pumping and Drip Irrigation Systems

The solar–powered pumping system comprised 40 solar cells (JKM 250P-60) placed in two groups of 20 modules each, which were connected in series before being connected together in parallel (Figure 1). Every solar module measured 165 cm length, 99.2 cm in width and 4 cm in thickness. To collect the most sunlight, the solar cell system was directed toward the south. The 40 PV cells (250 W) generated enough energy required to operate the submersible pump, which supplied the required amount of water for the entire farm. This solar-powered irrigation system was built to irrigate around 10 hectares farm. Solar radiation fluctuated throughout the year, with maximum and minimum values of 7.1 and 3.8 kWh m^{-2} recorded in June and December, respectively. The solar power system was connected to a 10 kW power controller (PS9K2) with 98% overall efficiency. Water was delivered to either a drip irrigation system or a concrete water reservoir (10 m length × 10 m width × 5 m depth) by a 7.5 kW PUC-SJ30-7 submersible pump.

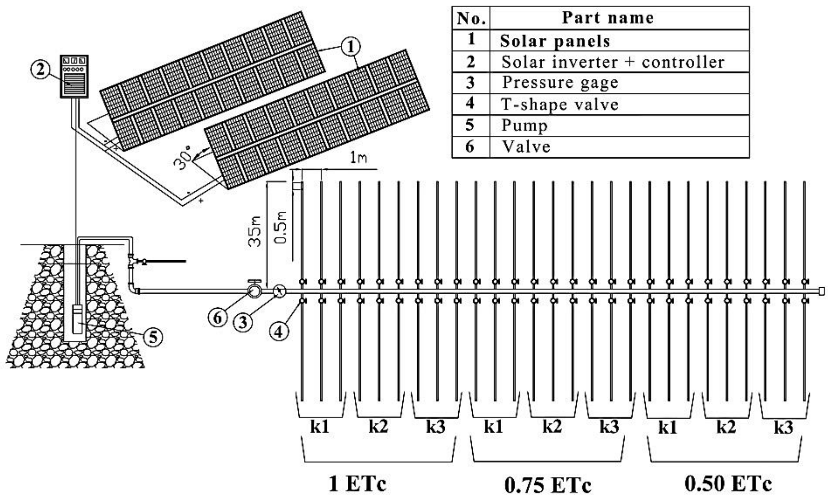

Figure 1. A schematic layout of the solar-powered pumping system connected with the drip irrigation network. K1, K2 and K3 are 150, 200, and 250 kg/ha of potassium treatments, respectively.

The drip irrigation system was used to irrigate the experimental plots, which consisted of 16 mm polyethylene lateral lines spaced at 1.0 m and emitters spaced at 0.5 m. In the system, a pressure differential tank was installed for the application of different fertilizers. An experimental unit was tested with three replicates using a split-plot design with nine 35 m long lateral lines with 4 L h^{-1} built-in emitters. The primary plots received irrigation treatments at random, while the secondary plots received K rates. Using Class A pan evaporation data, the applied irrigation water was determined based on reference evapotranspiration (ETo). With three replicates, the experiment was set as a split-plot design. The primary plots were watered at a certain pace, whereas the secondary plots were fertilized with potassium at a different rate. Squash plants were given nine various combinations of moisture (1.00, 0.75 and 0.50 ETc) and potassium rates (100, 150 and 250 kg K ha^{-1}). Starting two weeks after planting, potassium fertilization was applied weekly throughout the growing cycle, with the total amount of K varying based on the rate of each treatment. All experimental plots were fully irrigated for 21 days to guarantee the best germination ratio, and then various treatments were applied.

2.3. Calculation of Irrigation Water Requirements

According to the formula of Doorenbos and Kassam [62], reference evapotranspiration (*ETo*) was calculated according to the Class A pan evaporation technique as follows:

$$ETo = Epan \times Kpan \quad (1)$$

where *ETo* represents the reference evapotranspiration (mm d^{-1}), *Epan* represents the daily measured pan evaporation (mm d^{-1}), and *Kpan* is the pan coefficient, which was taken as 0.75 for the experimental location based on the local climatic conditions. According to Vermeiren and Jopling [63], the total irrigation water applied was calculated as follows:

$$AIW = \frac{ETo \times Kr \times I}{Ea} \quad (2)$$

where *AIW* represents the total depth of applied water, mm; *ETo* the reference evapotranspiration, mm day^{-1}; and the reduction factor, *Kr*, is influenced by the type of ground cover. According to James [64], this was assumed to be 1.0 (spacing between drip lines was <1.8 m). E_a is the drip irrigation system efficiency, which was assumed to be on average 0.8. I is the irrigation interval, days.

Irrigation time was identified before each irrigation event according to Ismail [65] as follows:

$$T = \left(\frac{AIW \times A}{q}\right) \quad (3)$$

where *T* is the duration of irrigation (h), *A* is the area sprayed by each emitter (m^2), and *q* is the discharge rate of the emitters (h^{-1} L).

According to the previous equations, the total amounts of water applied to different treatments in both investigated seasons were 371 and 308 mm for 1.00 ETc for the spring and fall seasons, respectively. The watering regimes of 0.75 and 0.50 ETc were then identified as percentages of 1.00 ETc for both seasons.

2.4. Determination of Squash Seed Yield and Chlorophyll Meter

At harvest, a 4 m^2 area from each treatment was collected to assess the overall production of squash seeds. Concurrent with collecting spectra reflectance from the squash canopy, we also measured the Chlm at the leaves. Each treatment's Chlm was measured with the use of a handheld SPAD chlorophyll meter (Konica-Minolta, Osaka, Japan).

2.5. Water-Use Efficiency

The following equation was implemented to determine water-use efficiency:

$$WUE = \frac{squash\ seed\ yield\ (\mathrm{kg\ ha^{-1}})}{applied\ irrigation\ water\ (\mathrm{m^3\ ha^{-1}})} \quad (4)$$

2.6. Potassium-Use Efficiency (KUE)

Potassium-use efficiency represents the ratio between squash seed yield and the entire amount of potassium added to the crop over the growing season, and was calculated as follows:

$$KUE = \frac{Y}{K} \quad (5)$$

where *KUE* represents the potassium-use efficiency, kg of squash seeds (kg K_2O_5)$^{-1}$; *Y* refers to the seed squash yield in kg ha^{-1} in a certain treatment; and *K* is the applied amount of K_2O_5 to the same treatment.

2.7. Reflectance Measurement Acquisition and Selection of Spectral Reflectance Indices

The spectra of squash plants' canopies were measured with a spectroradiometer from ASD that had a field of view of 3.5°. Because of the need for a wider scanning area, the detector was mounted on the end of a telescopic pole and maintained at a fixed height of about 1.25 m above the ground. The spectrometer could measure light with a wavelength of from 350 nm to 1075 nm. On cloud-free days between 11:30 to 13:30 h GMT, spectra were acquired from crop canopies under sun radiation. The spectrum reflectance of the sensor was calibrated using a white spectralon. Processed spectra were then used to derive different SRI$_s$. Table 3 lists some of the most widely used SRI$_s$ as well as the method for calculating, along with references. Eighteen SRIs, including the six most widely used SRI$_s$ and twelve freshly advanced three-band (3-D) SRIs, were examined (Table 3). Statistics were displayed on contour maps as determination coefficients (R^2) between four measured parameters (KUE, Chlm, WUE, and SY) with three-band SRIs (Figure 2). These indices were calculated by integrating potentials at any three wavelengths from a spectrum region ranging from 390 to 750 nm. According to Elsayed et al. [66], three-dimensional spectral reflectance maps were created. The provided maps are critical for establishing the optimal spectral region with feasible wavelengths and understanding the significance of three-band SRIs (Table 3).

Table 3. Several SRI indices explored in this study are described.

SRIs	Formula	References
Published SRIs		
$NDI_{780,550}$	$(R_{780} - R_{550})/(R_{780} + R_{550})$	[67]
Normalized chlorophyll index (NCI)	$(R_{750} - R_{678})/(R_{750} + R_{678})$	[68]
Normalized difference index ($NDI_{970,670}$)	$(R_{970} - R_{670})/(R_{970} + R_{670})$	[66]
Normalized water index 1 (NWI-1)	$(R_{970} - R_{900})/(R_{970} + R_{900})$	[69]
Normalized water index 3 (NWI-3)	$(R_{970} - R_{880}/(R_{970} + R_{880})$	[70]
Normalized water index 41 (NWI-4)	$(R_{970} - R_{920}/(R_{970} + R_{920})$	[71]
Newly three-band SRIs		
Normalized difference index (NDI)		
$NDI_{558,646,708}$	$(R_{558} - R_{646} - R_{708})/(R_{558} + R_{646} + R_{708})$	This work
$NDI_{538,708,648}$	$(R_{538} - R_{708} - R_{648})/(R_{538} + R_{708} + R_{648})$	
$NDI_{558,644,708}$	$(R_{558} - R_{644} - R_{708})/(R_{558} + R_{644} + R_{708})$	
$NDI_{744,746,738}$	$(R_{744} - R_{746} - R_{738})/(R_{744} + R_{746} + R_{738})$	
$NDI_{704,580,712}$	$(R_{704} - R_{580} - R_{712})/(R_{704} + R_{580} + R_{712})$	
$NDI_{704,712,582}$	$(R_{704} - R_{712} - R_{582})/(R_{704} + R_{712} + R_{582})$	
$NDI_{602,598,600}$	$(R_{602} - R_{598} - R_{600})/(R_{602} + R_{598} + R_{600})$	
$NDI_{644,630,652}$	$(R_{644} - R_{630} - R_{652})/(R_{644} + R_{630} + R_{652})$	
$NDI_{648,662,624}$	$(R_{648} - R_{662} - R_{624})/(R_{648} + R_{662} + R_{624})$	
$NDI_{670,628,392}$	$(R_{670} - R_{628} - R_{392})/(R_{670} + R_{628} + R_{392})$	
$NDI_{572,558,602}$	$(R_{572} - R_{5508} - R_{602})/(R_{572} + R_{558} + R_{602})$	
$NDI_{670,630,392}$	$(R_{670} - R_{630} - R_{392})/(R_{670} + R_{630\,+}\, R_{392})$	

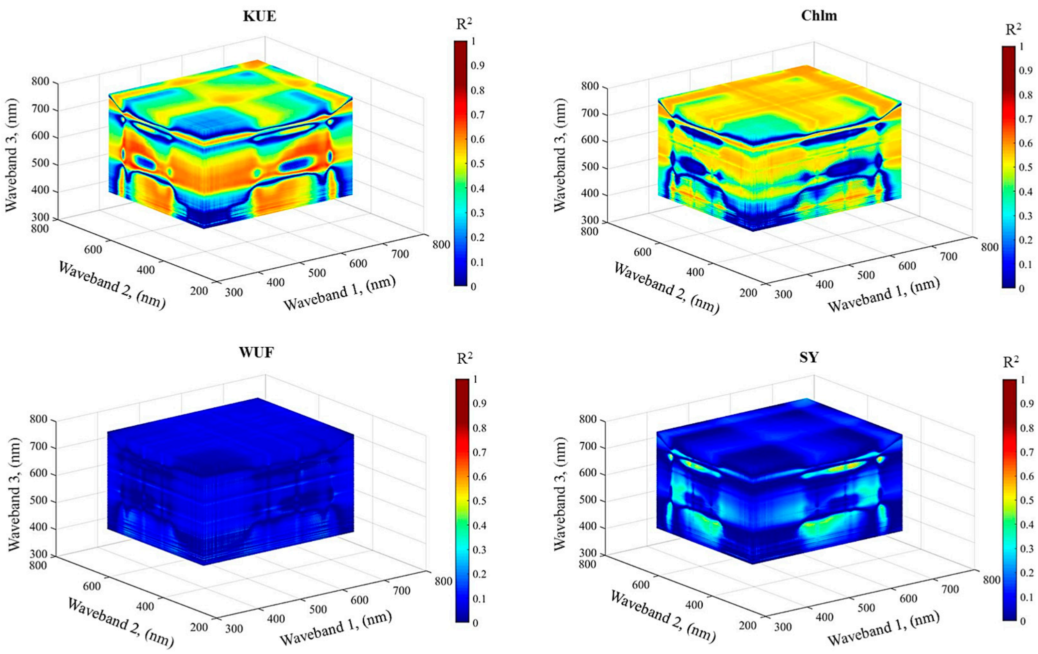

Figure 2. Correlation matrices displaying estimated (R^2) values for all potential three-band spectral combinations with potassium-use efficiency (KUE), chlorophyll meter (Chlm), water-use efficiency (WUE), and seed yield (SY) of squash across two successive seasons (spring and fall seasons).

2.8. Decision Tree (DT)

Decision tree induction is the process of training decision trees using class-labelled training tuples. A decision tree is a tree structure like a flowchart. The DT algorithm is composed of several nodes, each of which has a root, a leaf, and a decision. The root node is the one that starts the tree, and the decision nodes are the ones that are responsible for deciding what to do next, which means going from one node to another. The decision nodes are responsible for producing the leaf nodes. While some decision tree algorithms are limited to producing binary trees (having only two internal nodes), others are able to produce more complex trees [72]. As a result of their frequent usage in research [73], maximum depth (Md), maximum leaf nodes (Mln), and minimum sample leaf (S) were taken into consideration during training. For Md, Ms, and Mln, the parameter values were (1, 3, 5, 7), (2, 4, 6, 8), and (none, 10, 20, 30), respectively. By concentrating on these hyperparameters, we adjusted the model. In general, the model was supplied with the various characteristics at random during the first iteration, the low-level parameters were eliminated after each iteration, and the excellent parameters were retained with regard to the highest contribution. Then, all model outcomes were evaluated to choose high-quality parameters with a low model loss to accurately assess squash properties under moisture- and potassium-deficit stress. The DT can be easily transformed into regression rules. Because it does not need domain expertise or parameter setting, building decision tree regressors is ideal for exploratory knowledge discovery. The DTs used in this model are capable of handling high-dimensional input with accuracy. The DT models were based on spectral bands, SRIs and data fusion of both spectral bands, and SRIs were used to predict the four investigated traits (KUE, Chlm, WUE and SY) of squash.

2.9. Datasets and Software for Data Analysis

About 54 samples were utilized for training and validation; of these, 41 samples (or 80%) were used to exercise and test the regression model. However, the remaining 10 instances (or 20%) were employed to gauge the model's performance by contrasting projected and measured values. Before training, to correct for size disparities across various features, normalization was converted across individual features. By removing the minimal spectral data and dividing the difference between the highest and lowest feature values, feature normalization was calculated. Then, the model was trained and validated using a leave-one-out cross-validation (LOOCV) method. In each trial, LOOCV utilized the remaining data for training while excluding one sample for validation. This approach can lessen over-fitting and provide a more precise evaluation of the model's predictive power [73]. Data analysis, model construction, and data preparation were all carried out using Python 3.7.3 software. Research was conducted on the DT module, which is a part of the Scikit-learn package, version 0.20.2. This was carried out in order to finish the regression tasks. The examination of the data was carried out on a machine with an Intel Core i7–3630QM processor running at 2.4 GHz and 8 gigabytes of RAM.

2.10. Model Evaluation

The root mean square error (RMSE) and the coefficient of determination (R^2) are two statistical metrics that are applied in order to evaluate the efficacy of a regression model [74,75]. All the parameters that are being described are as follows: the term "F_{act}" refers to the actual value that was computed in the laboratory; "F_p" stands for the value that was predicted or simulated; "N" represents for the total number of data points; and "F_{ave}" indicates the value that was averaged out over all the data points.

Root mean square error:

$$\text{RMSE} = \sqrt{\frac{1}{N}\sum_{i=1}^{N}\left(F_{act} - F_{p}\right)^2} \quad (6)$$

Coefficient of determination:

$$R^2 = \frac{\sum\left(F_{act} - F_p\right)^2}{\sum\left(F_{act} - F_{ave}\right)^2} \tag{7}$$

2.11. Statistical Analysis

Combined analysis of variance across the two seasons was performed after performing the homogeneity test. The analysis of variance (ANOVA) of the split plot design was performed with irrigation regime (I) as the main-plot treatment in three levels, and potassium fertilizer (K) as a subplot factor in three rates, with three replicates for each level. Statistical analysis included analysis of variance (degrees of freedom (df), F-values, and significance level) of the effect of year, irrigation level, potassium level, and their interaction on SY, Chlm, WUE, KUE and spectral indices of squash. Least-significant differences (LSD) values were calculated to test the significance of differences between means. The Duncan test was performed to examine the significant difference of measured characteristics and SRIs of squash under varied nitrogen levels. Mean values with the same letter did not differ significantly ($p \leq 0.05$). Simple regressions were used to calculate the association between the SRIs and the assessed attributes. The 0.05, 0.01 and 0.001 probability levels were used to establish the significance level of the coefficients of determination (R^2) for these relationships. Using the collected spectra, which comprised all wavelengths from all treatments, principal component analysis (PCA) was used to assess differences and distinguish the spectral responses of non-stressed and stressed squash plants. The spectra collected from each plot were averaged, and the overall mean spectrum was examined in PCA to initially observe differences in the spectral signature acquired from healthy and varying stressed treatments (moisture and potassium deficiency). The raw data for the nine different treatments were composed of 135 columns and more than a thousand rows; therefore, we averaged the data to compress it, given the large size of the raw data. The different statistical analysis and plotting were performed using SPSS 22 (SPSS Inc., Chicago, IL, USA) and Minitab v.14 (Minitab Inc., State college, PA, USA).

3. Results and Discussion

3.1. Effects of Irrigation Treatments and Potassium Fertilization

The impacts of various potassium fertilizer rates and irrigation levels on the four measured parameters (SY, Chlm, WUE, KUE) were quantified using the analysis of variance (ANOVA) as summarized in Table 4 and Table S1. For example, in both the spring and fall seasons, both stressors (moisture and potassium fertilization) had a significant impact on SY of squash ($p < 0.05$) in Table S1. In both investigated seasons, the interaction between moisture and potassium demonstrated significant effects on the total SY of squash in Table S1 and Table 4. The experimental plots served by the combination 1.00 ETc and 250 kg K_2O_5 ha^{-1} produced the greatest squash seed yields of 1093.7 Kg ha^{-1}. Generally, squash seed yield demonstrated remarkable significant difference among K_2O_5 fertilization rates for a given watering regime. Due to the basic role of K in controlling stomata opening, which controls the transpiration process, high levels of K_2O_5 may minimize the impact of water stress [76] since stomatal closure is mainly preceded by a quick release of K. Reduced squash seed yields obtained from low doses of K showed its critical role in photosynthesis, as a lack of K slows photosynthesis and so reduces carbohydrate accumulation [77,78]. Another effect of a K deficit in plants is that the stomata do not open perfectly, resulting in less carbon dioxide and hence lower photosynthesis intensity, which leads to lower yield. In this context, it can be inferred that determining the right K rate in conjunction with the optimum irrigation regime for growing squash crops could improve squash water-use efficiency while reducing total irrigation usage. The outcomes of this research regarding Applied Irrigation Water (AIW) are similar to those reported by Topcu et al. [79]. Because of the combination of water stress and K deficiency, the chlorophyll meter of squash plants was significantly influenced by both rates of moisture level and K fertilization amounts.

The Chlm decreased in relation to the full application of water and K levels during both investigated seasons. The greatest chlorophyll content of 42.1 (SPAD values) was noticed with treatments that received the highest irrigation regime and 250 kg K ha^{-1} across two seasons (Table 4). In non-stressed plots, all K fertilization rates enhanced the Chlm. Our results showed that moisture-induced stress caused serious impairment of growth–related properties in terms of chlorophyll. Plant chlorophyll content was seen by Anjum et al. [80] as an indicator of water-induced stress owing to photo-oxidation. As a result of a decline in chlorophyll content due to water stress, photosynthesis slows dramatically, resulting in stunted plant development and significantly reduced output. The decrease in chlorophyll a level is particularly noticeable under deficit irrigation settings. The results reported by Mafakheri et al. [81] confirmed that chlorophyll concentration decreased dramatically with increasing water stress. All K fertilisation rates improved the Chlm in unstressed plots.

Table 4. Means and standard deviations of four parameters (potassium-use efficiency (KUE), chlorophyll meter (Chlm), water-use efficiency (WUE), and seed yield (SY) under interaction effect of irrigation regime and potassium fertilization rate across spring and fall seasons.

Season	**Irrigation Treatment**	**K Fertilization, kg ha^{-1}**			**Mean**
		150	**200**	**250**	
	1.00 ETc	811.5 ± 18.55 ^{c}	979.1 ± 16.77 ^{b}	1093.7 ± 24.12 ^{a}	961.4 ± 119.4 ^{A}
SY	0.75 ETc	466.3 ± 30.99 ^{g}	629.4 ± 140.87 ^{e}	960.3 ± 19.85 ^{b}	685.3 ± 223.5 ^{B}
	0.50 ETc	518.8 ± 15.99 ^{f}	544.6 ± 27.53 ^{f}	691.8 ± 96.55 ^{d}	585.1 ± 98.8 ^{C}
Mean		598.9 ± 158.1 ^{c}	717.7 ± 209.9 ^{b}	915.3 ± 181.1 ^{a}	
	1.00 ETc	32.1 ± 1.90 ^{d}	39.4 ± 1.73 ^{b}	42.1 ± 3.08 ^{a}	37.8 ± 4.59 ^{A}
Chlm	0.75 ETc	29.5 ± 1.69 ^{e}	31.9 ± 3.19 ^{d}	39.0 ± 2.91 ^{b}	33.5 ± 5.00 ^{B}
	0.50 ETc	28.4 ± 1.22 ^{e}	18.9 ± 0.83 ^{f}	34.8 ± 4.45 ^{c}	27.3 ± 7.39 ^{C}
Mean		29.9 ± 6.3 ^{c}	30.0 ± 8.9 ^{b}	38.6 ± 4.0 ^{a}	
WUE	1.00 ETc	0.241 ± 0.02 ^{e}	0.290 ± 0.03 ^{c}	0.325 ± 0.03 ^{b}	0.285 ± 0.04 ^{C}
	0.75 ETc	0.176 ± 0.02 ^{f}	0.233 ± 0.03 ^{e}	0.362 ± 0.03 ^{a}	0.257 ± 0.08 ^{B}
	0.50 ETc	0.269 ± 0.03 ^{d}	0.281 ± 0.02 ^{c}	0.354 ± 0.02 ^{a}	0.301 ± 0.05 ^{A}
Mean		0.228 ± 0.05 ^{c}	0.268 ± 0.04 ^{b}	0.347 ± 0.03 ^{a}	
	1.00 ETc	5.4 ± 0.12 ^{a}	4.9 ± 0.08 ^{b}	4.4 ± 0.10 ^{c}	4.893 ± 0.44 ^{A}
KUE	0.75 ETc	3.1 ± 0.21 ^{f}	3.2 ± 0.70 ^{f}	3.8 ± 0.08 ^{d}	3.365 ± 0.54 ^{B}
	0.50 ETc	3.5 ± 0.11 ^{e}	2.7 ± 14 ^{g}	2.8 ± 0.39 ^{g}	2.982 ± 0.40 ^{C}
Mean		4.0 ± 1.05 ^{a}	3.6 ± 1.05 ^{c}	3.7 ± 0.72 ^{b}	

Different letters in the same column indicate that means are significantly different ($p \leq 0.05$) according to Duncan's multiple range at 0.05 levels. Uppercase letters refer to the significance between the mean values of irrigation regime levels and lowercase letters refer to the significance between the mean values of potassium fertilizer levels.

Our findings demonstrated that chlorophyll-related properties associated with growth were severely compromised by moisture-induced stress. Chlorophyll concentration in plants was thought to be a sign of water-induced stress brought on by photo-oxidation by Anjum et al. [80]. Plants that are under water stress have lower chlorophyll concentrations, which significantly reduces photosynthesis and lowers plant growth and yield. The reduction in chlorophyll content is more pronounced when irrigation is insufficient. According to the findings of Mafakheri et al. [81], the chlorophyll content significantly decreased with increased water stress.

As seen in Table 4, the comparison of means for different treatments demonstrated that higher potassium fertilization rates produced higher WUE regardless of the watering regime. At all watering regimes (1.00, 0.75 and 0.50 ETc), the 150 kg potassium rate led to less WUE. The greatest WUE of 0.362 kg/m^3 was recorded with the combination of 250 kg K_2O_5 and 0.75 ETc. The significant effect of water stress on KUE is apparent, as shown in Table 5. When comparing the means of various combinations, the watering regime of 1.00 ETc produced higher KUE across two seasons with 5.41 kg squash seeds/kg K_2O_5 in comparison to 0.75 and 0.5 ETc.

Table 5. Means and standard deviations of spectral reflectance indices under interaction effects of irrigation regime and potassium fertilization rate across spring and fall seasons.

Treatments	$NDI_{780,550}$	NCI	$NDI_{970,670}$	NWI-1	NWI-3	NWI-4	$NDI_{558,646,708}$	$NDI_{538,708,648}$	$NDI_{558,644,708}$
1.00 ETc, 150K	0.645 ± 0.017^{a}	0.856 ± 0.010^{a}	0.859 ± 0.008^{a}	-0.020 ± 0.011^{b}	$-0.022 \pm 0.012^{b,c}$	-0.018 ± 0.007^{b}	-0.337 ± 0.009^{f}	-0.357 ± 0.012^{g}	-0.339 ± 0.010^{e}
1.00 ETc, 200K	0.601 ± 0.024^{b}	0.809 ± 0.047^{b}	0.807 ± 0.055^{b}	-0.022 ± 0.017^{b}	$-0.023 \pm 0.018^{b,c}$	-0.018 ± 0.012^{b}	-0.328 ± 0.006^{e}	-0.347 ± 0.006^{f}	-0.331 ± 0.007^{d}
1.00 ETc, 250K	0.560 ± 0.044^{c}	0.809 ± 0.066^{b}	0.805 ± 0.074^{b}	-0.022 ± 0.016^{b}	-0.024 ± 0.018^{c}	-0.019 ± 0.012^{b}	-0.324 ± 0.009^{e}	-0.346 ± 0.008^{f}	-0.327 ± 0.009^{d}
0.75 ETc, 150K	0.532 ± 0.025^{c}	0.812 ± 0.039^{b}	0.805 ± 0.048^{b}	-0.031 ± 0.020^{c}	-0.03 ± 0.022^{d}	-0.027 ± 0.015^{b}	-0.307 ± 0.005^{d}	-0.329 ± 0.007^{e}	-0.311 ± 0.005^{c}
0.75 ETc, 200K	0.349 ± 0.069^{e}	$0.735 \pm 0.018^{c,d}$	$0.720 \pm 0.021^{c,d}$	-0.022 ± 0.012^{b}	-0.023 ± 0.014^{c}	-0.019 ± 0.007^{b}	$-0.293 \pm 0.005^{b,c}$	-0.318 ± 0.007^{d}	-0.298 ± 0.004^{b}
0.75 ETc, 250K	0.215 ± 0.045^{g}	0.606 ± 0.063^{e}	0.576 ± 0.066^{e}	-0.022 ± 0.013^{b}	-0.024 ± 0.014^{c}	-0.019 ± 0.009^{b}	-0.294 ± 0.012^{c}	$-0.316 \pm 0.019^{c,d}$	-0.300 ± 0.012^{b}
0.50 ETc, 150K	0.302 ± 0.035^{f}	0.709 ± 0.059^{d}	0.690 ± 0.067^{d}	-0.021 ± 0.010^{b}	$-0.022 \pm 0.010^{b,c}$	-0.019 ± 0.006^{b}	-0.287 ± 0.008^{b}	$-0.310 \pm 0.009^{b,c}$	-0.293 ± 0.009^{b}
0.50 ETc, 200K	0.340 ± 0.138^{e}	0.747 ± 0.048^{c}	0.735 ± 0.056^{c}	-0.016 ± 0.010^{a}	-0.018 ± 0.012^{a}	-0.017 ± 0.005^{a}	-0.286 ± 0.013^{a}	-0.299 ± 0.015^{a}	-0.288 ± 0.012^{a}
0.50 ETc, 250K	0.467 ± 0.047^{d}	0.811 ± 0.018^{b}	0.808 ± 0.020^{b}	-0.019 ± 0.010^{b}	$-0.020 \pm 0.012^{a,b}$	-0.017 ± 0.006^{b}	$-0.287 \pm 0.018^{a,b,c}$	$-0.303 \pm 0.016^{a,b}$	-0.291 ± 0.017^{a}
	$NDI_{744,746,738}$	$NDI_{704,580,712}$	$NDI_{704,712,582}$	$NDI_{602,598,600}$	$NDI_{644,630,652}$	$NDI_{648,662,624}$	$NDI_{670,628,392}$	$NDI_{572,558,602}$	$NDI_{670,630,392}$
1.00 ETc, 150K	-0.326 ± 0.000^{a}	-0.366 ± 0.005^{f}	-0.363 ± 0.005^{f}	-0.341 ± 0.003^{e}	-0.346 ± 0.003^{c}	$-0.365 \pm 0.014^{b,c}$	$-0.417 \pm 0.018\ a^{b}$	$-0.317 \pm 0.001^{c,d}$	$-0.410 \pm 0.016^{a,b}$
1.00 ETc, 200K	-0.327 ± 0.001^{a}	-0.361 ± 0.008^{e}	-0.358 ± 0.007^{e}	-0.339 ± 0.001^{c}	-0.344 ± 0.004^{c}	-0.361 ± 0.009^{ab}	$-0.410 \pm 0.012^{a,b}$	-0.319 ± 0.002^{d}	$-0.402 \pm 0.011^{a,b}$
1.00 ETc, 250K	-0.328 ± 0.001^{b}	-0.347 ± 0.018^{d}	-0.343 ± 0.017^{d}	-0.339 ± 0.001^{c}	-0.340 ± 0.003^{b}	-0.361 ± 0.004^{b}	-0.402 ± 0.026^{a}	-0.318 ± 0.002^{d}	-0.395 ± 0.028^{a}
0.75 ETc, 150K	-0.328 ± 0.001^{b}	-0.344 ± 0.004^{d}	-0.341 ± 0.004^{d}	-0.341 ± 0.001^{de}	-0.340 ± 0.002^{b}	-0.365 ± 0.004^{b}	$-0.432 \pm 0.027^{b,c}$	-0.314 ± 0.002^{b}	$-0.425 \pm 0.032^{b,c}$
0.75 ETc, 200K	-0.331 ± 0.000^{d}	-0.316 ± 0.004^{b}	-0.313 ± 0.004^{b}	$-0.339 \pm 0.001^{b,c}$	-0.340 ± 0.003^{b}	-0.357 ± 0.003^{b}	-0.461 ± 0.023^{d}	$-0.312 \pm 0.001^{a,b}$	-0.454 ± 0.028^{d}
0.75 ETc, 250K	-0.333 ± 0.001^{f}	-0.309 ± 0.007^{a}	-0.307 ± 0.007^{a}	-0.336 ± 0.001^{a}	-0.340 ± 0.002^{b}	-0.348 ± 0.012^{c}	-0.417 ± 0.023^{b}	-0.316 ± 0.002^{c}	$-0.408 \pm 0.044^{a,b}$
0.50 ETc, 150K	-0.332 ± 0.000^{e}	-0.308 ± 0.005^{a}	-0.305 ± 0.005^{a}	-0.338 ± 0.001^{b}	-0.339 ± 0.002^{b}	-0.372 ± 0.003^{d}	-0.481 ± 0.022^{d}	-0.311 ± 0.002^{a}	-0.474 ± 0.025^{d}
0.50 ETc, 200K	-0.331 ± 0.001^{d}	-0.319 ± 0.008^{b}	-0.316 ± 0.008^{b}	-0.339 ± 0.002^{c}	-0.339 ± 0.005^{ab}	-0.356 ± 0.015^{e}	-0.475 ± 0.018^{d}	-0.313 ± 0.001^{b}	-0.471 ± 0.022^{d}
0.50 ETc, 250K	-0.330 ± 0.000^{c}	-0.335 ± 0.004^{c}	-0.332 ± 0.003^{c}	$-0.340 \pm 0.001^{c,d}$	-0.335 ± 0.004^{a}	-0.361 ± 0.012^{f}	-0.456 ± 0.027^{d}	-0.314 ± 0.003^{b}	$-0.450 \pm 0.028^{c,d}$

Different letters in the same column indicate that means are significantly different ($p \leq 0.05$) according to Duncan's multiple range at 0.05 levels.

3.2. *Effects of Irrigation Treatments and Potassium Fertilization on Published and Newly Spectral Reflectance Indices*

Irrigation treatments and potassium fertilisation had a general impact on SRIs. Numerous biophysical and biochemical traits of vegetation canopies are significantly altered by water stress in general. Fortunately, these modifications cause significant shifts in the canopy's spectral signatures across the entire spectrum at particular wavelengths [82–84]. The spectral reflectance of the plant canopy was found to be directly and indirectly affected by water stress and other fertilizers, such as potassium. Changes in leaf and plant properties, such as internal leaf structure, leaf pigments, and biomass, are connected to the indirect impacts and have a large impact on the spectral signature in the visible and near-infrared ranges. Variations in canopy water content cause alterations in spectral reflectance at the SWIR range and to certain wavelengths in the NIR spectrum region that can enter the leaves more deeply [85,86]. Considering the information above, in this work, we assessed how different SRIs, which combine different bands from the spectrum regions of VIS, red-edge, and NIR, responded to various irrigation schedules and potassium fertilization. According to our findings, all SRIs except for those with NWI-1, NWI-3, and NWI-4 demonstrated statistically significant differences among all treatments for squash in (Table 5). Additionally, all SRIs demonstrated statistically significant differences across year, irrigation level, potassium level, and their interaction in Table S2.

There were significant differences in the new three-band and published SRI values at various potassium fertilizer and irrigation levels (Table 5, Tables S1a, S2b and S3c), which may have been caused by wide variations in measured parameter values (Table 4). Quantitative analyses, for instance, showed that the mean values of the three-band SRIs, such as $NDI_{780,550}$, NCI and $NDI_{970,670}$ in Table 5, showed a substantial change from -0.3571 to -0.2994, from -0.3393 to -0.2881, and from -0.3266 to -0.3326, respectively. Additionally, the mean values of the published SRIs, such as $NDI_{538,708,648}$, $NDI_{558,644,708}$ and $NDI_{744,746,738}$ in Table 5 showed a substantial change from 0.215 to 0.6447, from 0.6059 to 0.8563, and from 0.5756 to 0.8589, respectively. SRI readings that gradually rise or decrease are linked to changes in the metrics measuring. These results also show that the reflectance of the plant canopy of the light spectrum regions at VIS, red-edge, and NIR was significantly affected by the irrigation regimes and potassium fertilizer levels. As a result, using the effective wavelengths selected from these three spectral regions, the resulting SRIs may provide a means of inferentially assessing the four evaluated parameters.

3.3. Assessment of the Measured Parameters via Comparison of Previously Published and Newly Developed Three-Band SRIs

The correlations between these four metrics of squash and the newly constructed three-band SRIs are shown in Table 6. Most of the published SRIs had weak relationships with the four investigated parameters with R^2 values varied from 0.00 to 0.73. Three-band SRIs which presented significant relationships with four parameters had R^2 values varying from 0.46 to 0.85, from 0.20 to 0.87, from 0.22 to 0.25, and from 0.21 to 0.80 for KUE, Chlm, WUE and SY, respectively, throughout the two seasons. According to the findings, the novel three-band indices derived from VIS, red-edge, and NIR wavelengths are sensitive estimators of the four traits investigated in the present research. $NDI_{558,646,708}$, $NDI_{538,708,64}$, and $NDI_{558,644,708}$ showed the highest R^2 which varied from 0.71 to 0.85 for KUE. $NDI_{744,746,738}$, $NDI_{704,580,712}$, and $NDI_{704,712,582}$ showed the highest R^2 ranging from 0.52 to 0.87 for Chlm, $NDI_{602,598,600}$, and $NDI_{644,630,652}$, and $NDI_{648,662,624}$ showed the highest R^2 ranging from 0.10 to 0.27 for Chlm; and $NDI_{670,628,392,}$ $NDI_{572,558,602}$ and $NDI_{670,630,392}$ showed the highest R^2 varying from 0.53 to 0.80 for SY throughout both seasons. However, across both seasons, for example, $NDI_{558,646,708}$ presented the highest R^2 of 0.75 for KUE, $NDI_{744,746,738}$ presented the highest R^2 of 0.65 for Chlm, $NDI_{602,598,600}$ presented the highest R^2 of 0.25 for WUE, and $NDI_{670,628,392}$ presented the highest R^2 of 0.64 for SY of squash.

Table 6. Relationships of linear regression of four parameters (potassium-use efficiency (KUE), chlorophyll meter (Chlm), water-use efficiency (WUE), and seed yield (SY)) with several SRIs of squash expressed as determination coefficients.

	Spring				Fall				Both Seasons			
SRIs	**KUE**	**Chlm**	**WUE**	**SY**	**KUE**	**Chlm**	**WUE**	**SY**	**KUE**	**Chlm**	**WUE**	**SY**
$NDI_{780,550}$	0.42 ***	0.54 ***	0.03	0.16	0.73 ***	0.66 ***	0.09	0.08	0.53	0.55 ***	0.06	0.14
NCI	0.13	0.35 **	0.06	0.02	0.44 ***	0.55 ***	0.10	0.00	0.21	0.42 ***	0.05	0.00
$NDI_{970,670}$	0.14	0.37 **	0.06	0.03	0.46 ***	0.54 ***	0.08	0.00	0.23	0.43 ***	0.04	0.00
NWI-1	0.04	0.02	0.14	0.24	0.00	0.10	0.22 *	0.51 ***	0.03	0.00	0.12	0.08
NWI-3	0.02	0.02	0.13	0.20	0.00	0.11	0.22 *	0.59 ***	0.03	0.00	0.11	0.08
NWI-4	0.08	0.01	0.14	0.30	0.01	0.12	0.22 *	0.51 ***	0.04	0.00	0.14	0.07
$NDI_{558,646,708}$	0.78 ***	0.36 **	0.03	0.27 *	0.80 ***	0.28 *	0.00	0.58 ***	0.75 ***	0.31 *	0.02	0.36 **
$NDI_{538,708,648}$	0.71 ***	0.37 **	0.07	0.19 *	0.85 ***	0.15	0.00	0.70 ***	0.75 ***	0.27 *	0.03	0.33 **
$NDI_{558,644,708}$	0.77 ***	0.34 **	0.03	0.25 *	0.80 ***	0.26 *	0.00	0.59 ***	0.75 ***	0.30 *	0.01	0.35 **
$NDI_{744,746,738}$	0.52 ***	0.57 ***	0.01	0.24 *	0.77 ***	0.77 ***	0.14	0.09	0.61 ***	0.65 ***	0.04	0.13
$NDI_{704,580,712}$	0.50 ***	0.52 ***	0.00	0.35 **	0.69 ***	0.86 ***	0.19 *	0.05	0.55 ***	0.64 ***	0.02	0.16
$NDI_{704,712,582}$	0.51 ***	0.52 ***	0.00	0.36 **	0.70 ***	0.87 ***	0.18 *	0.05	0.56 ***	0.64 ***	0.02	0.18 *
$NDI_{602,598,600}$	0.02	0.10	0.26 *	0.11	0.18	0.58 ***	0.23 *	0.02	0.04	0.20	0.25 *	0.01
$NDI_{644,630,652}$	0.02	0.00	0.27 *	0.21	0.02	0.18 *	0.15	0.16	0.00	0.02	0.24 *	0.11
$NDI_{648,662,624}$	0.00	0.03	0.22 *	0.08	0.01	0.33 *	0.10	0.17	0.00	0.04	0.19 *	0.01
$NDI_{670,628,392}$	0.60 ***	0.25 *	0.05	0.53 ***	0.47 ***	0.01	0.02	0.80 ***	0.50 ***	0.09	0.01	0.64 ***
$NDI_{572,558,602}$	0.54 ***	0.13	0.10	0.61 ***	0.67 ***	0.10	0.06	0.66 ***	0.56 ***	0.09	0.04	0.64 ***
$NDI_{670,630,392}$	0.60 ***	0.26 *	0.05	0.53 ***	0.46 ***	0.01	0.01	0.79 ***	0.50 ***	0.08	0.01	0.64 ***

*, **, *** Significant at $p \leq 0.05$, $p \leq 0.01$ and $p \leq 0.001$ probability levels, respectively.

The information gleaned will be crucial for advancing endeavors to employ specific spectral devices for carrying out precise characteristic practices. Very little attention has been given to 3D contour maps created with three-band SRIs to evaluate these parameters at various potassium fertilizer rates and water regime levels. Because of their sensitivity to the assessment of complicated development variables, such as genotypes, growth phase, canopy features, and environment, indices based on wavelengths from a single band range make it difficult to reliably quantify plant attributes. Nonetheless, indices that incorporate bands from all three spectral bands are less saturated and less susceptible to a wide variety of plant characteristics, such as the leaf's interior structure and metabolic contents. This may help to explain why three-band SRIs were more accurate than two-band SRIs in estimating the four parameters. These outcomes support the earlier findings of Babar et al. [70] and Prasad et al. [69], which showed that crop yield could be predicted before the plant matured, while hyperspectral data demonstrated the potential to distinguish between moisture-related and K-deficiency-related stresses. Utilizing a variety of spectral indices, Kawamura et al. [87] assessed the soil phosphorus and potassium fertility status in pastures with legumes. The photochemical reflectance index was closely correlated with the phosphorus and potassium contents (PRI). Strong correlations between the potassium content of rice leaves and various vegetation indices were discovered in a study by Lu et al. [88]. Depending on the soil and crop conditions, there are different relationships between nutrient content and vegetation indices. The findings of a study on wheat by Pimstein et al. [89] showed the effectiveness of selected vegetation indices estimate wheat traits under potassium and phosphorus levels.

3.4. Differentiating Moisture and Potassium Deficiency Spectrally

The PCA was operated using all datasets in the spring and fall seasons to distinguish between moisture and potassium deficiency stress. Figures 3 and 4 illustrate the score plot of the PCA for datasets collected at the flowering stage of the squash crop. The figures demonstrate dissimilarities between non-stressed plants and those suffering from moisture and potassium deficiency stress. As shown in Figure 3b, the ideal bands were chosen, in which the first two PC explained 99.97% of the variance and accounted for 97.93% and 2.04% of the total spectral variation at PCI and PC2, respectively. As depicted in Figure 4b, the most effective bands were picked, accounting for 97.14% and 2.80%, respectively, of the total spectral variation at PCI and PC2, with 99.94% of the variance being characterized by the first two PCs. The spectra acquired from plots with high watering regimes were close to each other and were plotted in one quarter of the score plot. However, the spectral measurements collected from stressed plants tended to plot in a different quarter of the score plot, which may be attributed to lower leaf water content and chlorophyll content. As seen in Figure 3, for example, the arrow on the left side shows an increase in the potassium rate with the same watering regime (0.75 ETc). The arrow in the right side also demonstrates the same pattern (increasing potassium fertilization rate with the same watering regime, 1.0 ETc). The dissimilarities shown between non-stressed and stressed treatments may have been a result of remarkable variations in the biochemical and biophysical properties of squash plants. These variations could be useful in determining the time of sensitive periods to stress. The results further demonstrated the PCA loading plots proposed that spectra over the VIS range seem to be strongly associated with the level of stress, whereas the variations between the near-infrared spectra make it possible to differentiate both tested stressors. The results show that utilizing remotely sensed data to monitor plant status with greater leaved plants, such as squash, will enhance the efficiency of this technique. PCA score plots revealed that differentiating between moisture and potassium deficiency stress is possible, particularly when plants are subjected to severe stress. Other studies revealed that remotely sensed data would be useful for distinguishing sources of stress. For instance, Elmetwalli and Tyler [39] employed PCA to distinguish between nitrogen and water deficiency in maize and proved the potential of discriminating both stressors spectrally. Elmetwalli et al. [37] mentioned that the PCA score plot showed the feasibility of distinguishing between wheat plants which suffer from water and salinity stress.

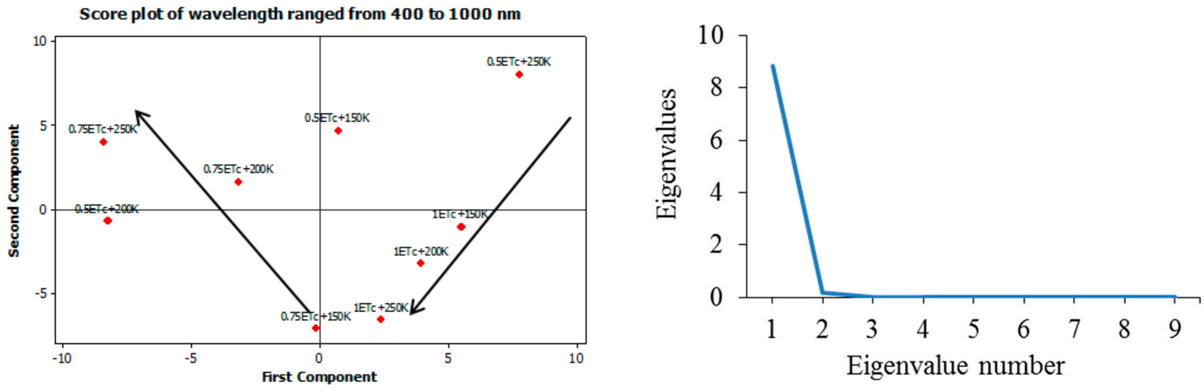

(**a**) (**b**)

Figure 3. The score plot of (**a**) PCA and (**b**) Eigenvalue number created for the spectral measurements acquired from non-stressed and stressed squash plants at the flowering stage in spring season. Treatment labels; 0.50 ETc + 150K (50% ETc watering regime and 150 kg K_2O_5/ha potassium fertilization rate).

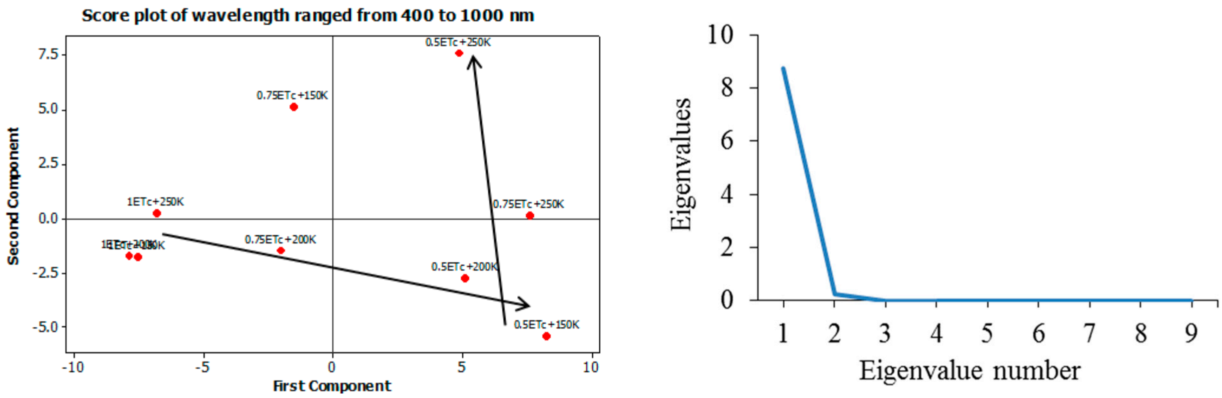

(**a**) (**b**)

Figure 4. The score plot of (**a**) PCA and (**b**) Eigenvalue number created for the spectral measurements acquired from non-stressed and stressed squash plants at the flowering stage in fall season. Treatment labels; 0.50 ETc + 150K (50% ETc watering regime and 150 kg K_2O_5/ha potassium fertilization rate).

3.5. Performance of Decision Tree Model for Predicting Four Squash Parameters

Although SRIs are a straightforward method for indirectly evaluating plant features, they only capture the relationships of the spectral reflectance value at a few wavelengths and ignore the rest of the information included in hyperspectral data. For evaluating plant attributes in varying environmental circumstances, SRI effectiveness is sometimes affected by the small number of wavelengths available for analysis [90,91]. This is due to the fact that SRIs become more sensitive to off-target qualities, such as differences in vegetation's physical and biological properties, when a selective wavelength is mixed in a certain formula. The precise estimate of plant features has been shown to be enhanced using spectral bands, SRIs, and combinations of spectral bands and SRIs, as well as the creation of data-driven models, such as DT.

To filter the highest variables, the DT model was used with the 3D-spectral indices (3D-SRIs), DT-based bands (DT-b), and the aggregate of all spectral characteristics (ASF), as shown in Table 7. These characteristics were effective for identifying squash crop characteristics. Table 7 demonstrates how the decision tree model was trained to predict the studied parameters (dependent variables) using the 3D-SRIs, DT-b, and ASF (independent variables). After that, the projected values were contrasted with the DT model's reserved values that were not used. The results of this study's analysis and comparison of multivariate methodologies show that doing so greatly increases predictability. Since validation data are not utilized in the building of the regression model, independent validation is the most trustworthy way for determining the model's accuracy. The findings showed that the DT-DT-b-30 was the most accurate prediction model, with a greater correlation between potassium and the standout features. This model's approximately 30 spectral characteristics are extremely important for forecasting KUE. Its outputs with R^2 for the training and validation sets were 0.967 (RMSE = 0.175) and 0.818 (RMSE = 0.284), respectively. For measuring Chlm, the DT-DT-b-20 model fared the best. In the training and validation datasets, the R^2 values were 0.993 (RMSE = 0.522) and 0.692 (RMSE = 2.321), respectively. The most accurate model (DT-SRIs-3) for identifying WUF had R^2 values of 0.576 and 0.447 and RMSE values of 0.039 and 0.035 for the training and validation datasets, respectively. The DT- SRIs-1 model scored better at forecasting SY than the others. The model's R^2 performance for the training and validation sets, respectively, was 0.799 (RMSE = 97.473) and 0.699 (RMSE = 87.656). According to Elsherbiny [92,93], who claim that the performance exceeded expectations, numerous training phases, searching high-level characteristics and tweaking model hyperparameters were necessary to update regression approaches for reliable prediction.

Table 7. Results of a decision tree model based on different features extracted from hyperspectral data.

Variable	Spectral Features	Optimal Parameters	Training		Validation	
		(Md, Ms, Mln)	R^2	RMSE	R^2	RMSE
KUE	a	(5, 2, 10)	0.97 ***	0.175	0.82 ***	0.284
	b	(3, 6, none)	0.84 ***	0.386	0.74 ***	0.372
	c	(5, 4, none)	0.96 ***	0.201	0.76 ***	0.330
Chlm	a	(5, 2, none)	0.99 ***	0.522	0.69 ***	2.321
	b	(7, 2, 30)	0.91 ***	1.840	0.60 ***	2.781
	c	(5, 2, none)	0.99 ***	0.555	0.52 ***	2.864
WUE	a	(7, 2, 10)	0.87 ***	0.021	0.35 **	0.037
	b	(3, 10, none)	0.58 ***	0.039	0.45 **	0.035
	c	(3, 10, none)	0.58 ***	0.039	0.41 **	0.039
Yield	a	(10, 8, none)	0.65 ***	129.480	0.19 *	148.946
	b	(3, 6, none)	0.80 ***	97.473	0.70 ***	87.656
	c	(3, 10, none)	0.80 ***	98.500	0.69 ***	90.031

Md is max depth, Ms is min samples leaf, and Mln is max leaf nodes. The symbols a, b, and c indicate DT-based bands, 3D-VIs, and the aggregation of all spectral features, respectively. *, **, and ***, statistically significant at $p \leq 0.05$, $p \leq 0.01$, and $p \leq 0.00$, respectively.

From the above mentioned results, it can be seen that the model's prediction accuracy is affected by the value and number of features. Table S3 shows a variety of choices for merging features and models that have the greatest influence on the prediction of quality attributes in squash crops. This table explains that there are unique characteristics of training models that have the lowest RMSEV value and perform well in predicting. Depending on the model used, the RMSEV value dropped with these specified features.

4. Conclusions

This investigation tested the potential of spectral reflectance measurements to determine squash properties and find dissimilarities between non-stressed and stressed squash plants. Few studies of this kind have produced three-dimensional contour maps employing SRIs to evaluate these characteristics across varying water regimes and potassium fertilizer rates. The results demonstrated the sensitivity of the newly constructed three-band SRIs for estimating the four squash parameters, with wavelengths spanning the visible (VIS), red-edge, and near-infrared (NIR) domains. The results showed that the newly built three-band SRIs, covering the visible (VIS), red-edge (RE), and near-infrared (NIR) spectral ranges, were sensitive enough to estimate the four tested squash parameters. The results further demonstrated that the PCA showed the ability to separate moisture induced stress from potassium deficiency stress at the flowering stage onwards. The DT model's prediction accuracy is affected by the value and number of features. The results of the models shows a variety of choices for merging features and models that have the greatest influence on the prediction of quality attributes in squash crops. The DT-SRIs-1 model scored better at forecasting SY than the others. The model's R^2 performance for the training and validation datasets, respectively, was 0.799 (RMSE = 97.473) and 0.699 (RMSE = 87.656). The overall results demonstrate that proximal reflectance sensing based on SRIs, as well as a DT model including spectral bands, SRIs or their combinations, could be used to estimate the four squash parameters under different levels of water regimes and potassium fertilization rates.

Supplementary Materials: The following supporting information can be downloaded at: https://www.mdpi.com/article/10.3390/horticulturae9010079/s1, Table S1. Statistical analysis, including analysis of variance (degrees of freedom (df), F-values, and significance level) of the effect of year, irrigation level, potassium level, and their interaction on seed yield; Table S2. Statistical analysis, including analysis of variance (degrees of freedom (df), F-values, and significance level) of the effect of year, irrigation level, potassium level, and their interaction on spectral indices of squash; Table S3. Ranking of the most significant spectral characteristics.

Author Contributions: Conceptualization, M.A.S.-E., A.N.T.; S.E. and A.H.E.; methodology, M.A.S.-E., O.E., S.E. and A.H.E.; software, M.A.S.-E., O.E., Z.M.Y., A.E.-D.O., M.E., S.E.-N., S.E. and A.H.E.; validation, M.A.S.-E., O.E., F.S.M., Z.M.Y., A.E.-D.O., A.N.T., S.E. and A.H.E.; formal analysis, M.A.S.-E., O.E., Z.M.Y., A.N.T., M.E., F.S.M., S.E. and A.H.E.; resources, M.A.S.-E., O.E., S.E.-N., M.E., S.E. and A.H.E.; data curation, M.A.S.-E., O.E., Z.M.Y., M.E., S.E. and A.H.E.; writing—original draft preparation, M.A.S.-E., O.E., S.E. and A.H.E.; writing—review and editing, M.A.S.-E., O.E., F.S.M., M.E., Z.M.Y., S.E.-N., A.N.T., A.E.-D.O., S.E. and A.H.E.; visualization, M.A.S.-E., M.E., F.S.M., Z.M.Y., S.E. and A.H.E.; supervision, S.E., A.N.T., M.E. and A.H.E.; project administration, S.E., A.H.E., A.N.T., M.E., S.E.-N. and A.E.-D.O.; funding acquisition, M.E., F.S.M., S.E.-N. and A.E.-D.O. All authors have read and agreed to the published version of the manuscript.

Funding: King Khalid University funded this work through the Large Groups Project under grant number L.G.P. 2/138/43.

Data Availability Statement: Data are presented in the article.

Acknowledgments: The authors extend their appreciation to the Deanship of Scientific Research at King Khalid University for funding this work through the Large Groups Project under grant number L.G.P. 2/138/43.

Conflicts of Interest: The authors declare no conflict of interest.

References

1. Rouphael, Y.; Colla, G. Growth, yield, fruit quality and nutrient uptake of hydroponically cultivated zucchini squash as affected by irrigation systems and growing seasons. *Sci. Hortic.* **2005**, *105*, 177–195. [CrossRef]
2. Qamar, R.; Khan, S.; Safdar, M.E.; Atique-ur-Rehman, R.A.; Abdul, R.A.; Javeed, H.M.R.; Nadeem, M.A.; Al-Yahyai, R.; Alkahtani, J. Seed priming with growth regulators modulates production, physiology and antioxidant defense of Indian squash (*Praecitrullus fistulosus*) under semi-arid conditions. *PLoS ONE* **2022**, *17*, e0265694. [CrossRef] [PubMed]
3. Farah, A.H.; Al-Ghobari, H.M.; Zin El-Abedin, T.K.; Alrasasimah, M.S.; El-Shafei, A.A. Impact of partial root drying and soil mulching on squash yield and water use efficiency in arid. *Agronomy* **2021**, *11*, 706. [CrossRef]
4. Bannayan, M.; Rezaei, E.E.; Alizadeh, A. Climatic suitability of growing summer squash (*Cucurbita pepo* L.) as a medicinal plant in Iran. *Not. Sci. Biol.* **2011**, *3*, 39–46. [CrossRef]
5. Bose, T.K.; Kabir, J.; Das, P.; Joy, P.P. *Tropical Horticulture*, 1st ed.; Naya Prakash: Calcutta, India, 2001; Volume 2, 771p.
6. Al-Omran, A.M.; Sheta, A.S.; Falatah, A.M.; Al-Harbi, A.R. Effect of drip irrigation on squash (*Cucurbita pepo*) yield and water-useefficiency in sandy calcareous soils amended with clay deposits. *Agric. Water Manag.* **2005**, *73*, 43–55. [CrossRef]
7. Hao, B.; Xue, Q.; Marek, T.H.; Jessup, K.E.; Hou, X.; Xu, W.; Bynum, E.D.; Bean, B.W. Radiation—Use efficiency, biomass production, and grain yield in two maize hybrids differing in drought tolerance. *J. Agron. Crop Sci.* **2016**, *202*, 269–280. [CrossRef]
8. Lin, K.H.; Kuo, W.S.; Chiang, C.M.; Hsiung, T.C.; Chiang, M.C.; Lo, H.F. Study of sponge gourd ascorbate peroxidase and winter squash superoxide dismutase under respective flooding and chilling stresses. *Sci. Hortic.* **2013**, *162*, 333–340. [CrossRef]

9. Ors, S.; Ekinci, M.; Yildirim, E.; Sahin, U. Changes in gas exchange capacity and selected physiological properties of squash seedlings (*Cucurbita pepo* L.) under well-watered and drought stress conditions. *Arch. Agron. Soil Sci.* **2016**, *62*, 1700–1710. [CrossRef]
10. Yildirim, E.; Ekinci, M.; Sahin, U.; Ors, S.; Turan, M.; Demir, I.; Dursun, A.; Kotan, R. Improved water productivity in summer squash under water deficit with PGPR and synthetic methyl amine applications. *Rhizosphere* **2021**, *20*, 100446. [CrossRef]
11. Ashraf, M. Inducing drought tolerance in plants: Some recent advances. *Biotechnol. Adv.* **2010**, *28*, 169–183. [CrossRef]
12. Kuslu, Y.; Sahin, U.; Kiziloglu, F.M.; Memis, S. Fruit yield and quality, and irrigation water use efficiency of summer squash drip-irrigated with different irrigation quantities in a semi-arid agricultural area. *J. Integrat. Agric.* **2014**, *13*, 2518–2526. [CrossRef]
13. Amer, K.H. Effect of irrigation method and quantity on squash yield and quality. *Agric. Water Manag.* **2011**, *98*, 1197–1206. [CrossRef]
14. Martinetti, L.; Paganini, F. Effect of organic and mineral fertilisation on yield and quality of zucchini. *Acta Hortic.* **2006**, *700*, 125–128. [CrossRef]
15. Alves, J.; Lima, A.; Suassuna, C.; Figueiredo, F.; da Silva, T.; Mesquita, E.; Cavalcante, L.; Mesquita, F. Growth and gas exchange of Cucurbita pepo L. under nitrogen and silicon fertilization. *J. Agric. Sci.* **2019**, *11*, 83. [CrossRef]
16. Bello, S.K.; AL-Solaimani, S.G.; Abo-Elyousr, K.A.M. Squash yield, water-use efficiency and nitrate accumulation as influenced by the application of humic acid, geobacillus stearothermophilus SSK-2018 and wheat straw in an arid land condition. *Horticulturae* **2022**, *8*, 588. [CrossRef]
17. Ajdary, K.; Singh, D.K.; Singh, A.K.; Khanna, M. Modelling of nitrogen leaching from experimental onion field under drip fertigation. *Agric. Water Manag.* **2007**, *89*, 15–28. [CrossRef]
18. Kalaivanan, D.; Selvakumar, G.; Hebbar, S.S. Effects of varying N, P and K concentrations on growth, biomass, yield and nutritional quality of zucchini squash grown under open and polyhouse soilless culture. *Indian J. Hortic.* **2020**, *77*, 100–106. [CrossRef]
19. Elsayed, S.; Barmeier, G.; Schmidhalter, U. Passive reflectance sensing and digital image analysis allows for assessing the biomass and nitrogen status of wheat in early and late tillering stages. *Front. Plant Sci.* **2018**, *9*, 1478. [CrossRef]
20. Elsayed, S.; El-Hendawy, S.; Khadr, M.; Elsherbiny, O.; Al-Suhaibani, N.; Alotaibi, M.; Tahir, M.U.; Darwish, W. Combining thermal and RGB imaging indices with multivariate and data-driven modeling to estimate the growth, water status, and yield of potato under different drip irrigation regimes. *Remote Sens.* **2021**, *13*, 1679. [CrossRef]
21. Elsayed, S.; El-Hendawy, S.; Khadr, M.; Elsherbiny, O.; Al-Suhaibani, N.; Dewir, Y.H.; Tahir, M.U.; Mubushar, M.; Darwish, W. Integration of spectral reflectance indices and adaptive Neuro-Fuzzy Inference System for assessing the growth performance and yield of potato under different drip irrigation regimes. *Chemosensors* **2021**, *9*, 55. [CrossRef]
22. Lu, S.; Lu, F.; You, W.; Wang, Z.; Liu, Y.; Omasa, K. A robust vegetation index for remotely assessing chlorophyll content of dorsiventral leaves across several species in different seasons. *Plant Methods* **2018**, *14*, 2–15. [CrossRef] [PubMed]
23. Niu, Y.X.; Zhang, L.Y.; Zhang, H.H.; Han, W.T.; Peng, X.S. Estimating above-ground biomass of maize using features derived from UAV-based RGB imagery. *Remote Sens.* **2019**, *11*, 1261. [CrossRef]
24. Lin, H.; Lin, K.; Huang, M.; Su, Y. Use of non-destructive measurements to identify cucurbit species (*Cucurbita maxima* and *Cucurbita moschata*) tolerant to Waterlogged conditions. *Plants* **2020**, *9*, 1226. [CrossRef] [PubMed]
25. Abdulridha, J.; Ampatzidis, Y.; Roberts, P.; Kakarla, S.C. Detecting powdery mildew disease in squash at different stages using UAV-based hyperspectral imaging and artificial intelligence. *Biosyst. Eng.* **2020**, *197*, 135–148. [CrossRef]
26. Elmetwalli, A.H.; El-Hendawy, S.; Al-Suhaibani, N.; Alotaibi, M.; Tahir, M.U.; Mubushar, M.; Hassan, W.M.; Elsayed, S. Potential of hyperspectral and thermal proximal sensing for estimating growth performance and yield of soybean exposed to different drip irrigation regimes under arid conditions. *Sensors* **2020**, *22*, 6569. [CrossRef]
27. El-Hendawy, S.E.; Al-Suhaibani, N.; Elsayed, S.; Hanssan, W.M.; Dewir, Y.H. Potential of the existing and novel spectral reflectance indices for estimating the leaf water status and grain yield of spring wheat exposed to different irrigation rates. *Agric. Water Manag.* **2019**, *217*, 356–373. [CrossRef]
28. Lobos, G.A.; Romero, S.; Escobar, A.; Estrada, F.; Caligari, P.D.S.; Poblete-Echeverria, C.; Ahumada, L.; Zuniga, M. Fast and non-distructive prediction of gas exchange in olive orchardes (*Olea europaea* L.) under different soil conditions. *Acta Hortic.* **2014**, *1057*, 329–334. [CrossRef]
29. Zhang, Q.; Li, Q.; Zhang, G. Rapid determination of leaf water content using VIS/NIR spectroscopy analysis with wavelength selection. *Int. J. Spectrosc.* **2012**, *27*, 93–105. [CrossRef]
30. Elsayed, S.; Rischbeck, P.; Schmidhalter, U. Comparing the performance of active and passive reflectance sensors to assess the normalized relative canopy temperature and grain yield of drought-stressed barley cultivars. *Field Crops Res.* **2015**, *177*, 148–160. [CrossRef]
31. Elsayed, S.; Elhoweity, M.; Ibrahim, H.H.; Dewir, Y.H.; Migdadic, H.M.; Schmidhalter, U. Thermal imaging and passive reflectance sensing to estimate the water status and grain yield of wheat under different irrigation regimes. *Agric. Water Manag.* **2017**, *189*, 98–110. [CrossRef]
32. Elsayed, S.; El-Hendawy, S.; Dewir, Y.H.; Schmidhalter, U.; Ibrahim, H.H.; Ibrahim, M.M.; Elsherbiny, O.; Farouk, M. Estimating the leaf water status and grain yield of wheat under different irrigation regimes using optimized two- and three-band hyperspectral indices and multivariate regression models. *Water* **2021**, *13*, 2666. [CrossRef]

33. El-Hendawy, S.; Dewir, Y.H.; Elsayed, S.; Schmidhalter, U.; Al-Gaadi, K.; Tola, E.; Refay, Y.; Tahir, M.U.; Hassan, W.M. Combining hyperspectral reflectance indices and multivariate analysis to estimate different units of chlorophyll content of spring wheat under salinity conditions. *Plants* **2022**, *11*, 456. [CrossRef] [PubMed]
34. Elmetwalli, A.H. Remote Sensing as a Precision Farming Tool in the Nile Valley, Egypt. Ph.D. Thesis, School of Biological and Environmental Sciences, University of Stirling, Stirling, UK, 2008.
35. Gnyp, M.L.; Miao, Y.; Yuan, F.; Ustin, S.L.; Yu, K.; Yao, Y.; Huang, S.; Bareth, G. Hyperspectral canopy sensing of paddy rice aboveground biomass at different growth stages. *Field Crops Res.* **2014**, *155*, 42–55. [CrossRef]
36. Kanke, Y.; Tubana, B.; Dalen, M.; Harrell, D. Evaluation of red and red edge reflectance based vegetation indices for rice biomass and grain yield prediction models in paddy fields. *Precis. Agric.* **2016**, *17*, 507–530. [CrossRef]
37. Elmetwalli, A.H.; Tyler, A.N. Estimation of maize properties and differentiating moisture and nitrogen deficiency stress via ground-based remotely sensed data. *Agric. Water Manag.* **2020**, *242*, 106413. [CrossRef]
38. Jin, X.; Wang, K.; Xiao, C.; Diao, W.; Wang, F. Comparison of two methods for estimation of leaf total chlorophyll content using remote sensing in wheat. *Field Crops Res.* **2012**, *135*, 24–29. [CrossRef]
39. Elmetwalli, A.H.; Tyler, A.N.; Hunter, P.D.; Salt, C.A. Detecting and distinguishing moisture and salinity induced stress in wheat and maize through in situ spectroradiometry measurements. *Remote Sens. Lett.* **2012**, *5*, 363–372. [CrossRef]
40. Elmetwalli, A.H.; Mazrou, Y.S.A.; Tyler, A.N.; Hunter, P.D.; Esherbiny, O.; Yassen, Z.M.; Elsayed, S. Assessing the efficiency of remote sensing and machine learning algorithms to quantify wheat characteristics in the Nile Delta Region of Egypt. *Agriculture* **2022**, *12*, 332. [CrossRef]
41. Martinez, M.; Ramos, A. Estimation of chlorophyll concentration in maize using spectral reflectance. In Proceedings of the 36th International Symposium on Remote Sensing of Environment, Berlin, Germany, 11–15 May 2015; Volume XL-7/W3, pp. 65–71.
42. Schlemmer, M.; Gitelson, A.; Schepers, J.; Ferguson, R.; Peng, Y.; Shanahan, J.; Rundquist, D. Remote estimation of nitrogen and chlorophyll content in maize at leaf and canopy levels. *Int. J. Appl. Earth Obs. Geoinf.* **2013**, *25*, 47–54. [CrossRef]
43. Kawamura, K.; Ikeura, H.; Phongchanmaixay, S.; Khanthavong, P. Canopy hyperspectral sensing of paddy fields at the booting stage and PLS regression can assess grain yield. *Remote Sens.* **2018**, *10*, 1249. [CrossRef]
44. Weber, V.S.; Araus, J.L.; Cairns, J.E.; Sanchez, C.; Melchinger, A.E.; Orsini, E. Prediction of grain yield using reflectance spectra of canopy and leaves in maize plants grown under different water regimes. *Field Crops Res.* **2012**, *128*, 82–90. [CrossRef]
45. Nguy-Robertson, A.; Gitelson, A.; Peng, Y.; Vina, A.; Arkebauer, T.; Rundquist, D. Green leaf area index estimation in maize andsoybean: Combining vegetation indices to achieve maximal sensitivity. *Agron. J.* **2012**, *104*, 1336–1347. [CrossRef]
46. Casadesús, J.; Villegas, D. Conventional digital cameras as a tool for assessingleaf area index and biomass for cereal breeding. *J. Integr. Plant Biol.* **2014**, *56*, 7–14. [CrossRef]
47. Elmetwalli, A.H.; Tyler, A.N.; Moghanm, F.S.; Alamri, S.A.; Eid, E.M.; Elsayed, S. Integration of radiometric ground-based data and high resolution QuickBird imagery with multivariate modeling to estimate maize traits in the Nile Delta of Egypt. *Sensors* **2021**, *21*, 3915. [CrossRef] [PubMed]
48. Thorp, K.R.; Wang, G.; Bronson, K.F.; Badaruddin, M.; Mon, J. Hyperspectral data mining to identify relevant canopy spectral features for estimating durum wheat growth, nitrogen status and grain yield. *Comput. Electron. Agric.* **2017**, *136*, 1–12. [CrossRef]
49. Tan, K.; Wang, S.; Song, Y.; Liu, Y.; Gong, Z. Estimating nitrogen status of rice canopy using hyperspectral reflectance combined with BPSO-SVR in cold region. *Chemom. Intell. Lab. Syst.* **2018**, *172*, 68–79. [CrossRef]
50. Dejonge, K.C.; Mefford, B.S.; Chavez, J.L. Assessing corn water stress using spectral reflectance. *Int. J. Remote Sens.* **2016**, *10*, 2294–2312. [CrossRef]
51. Genc, H.; Genc, L.; Turhan, H.; Smith, S.E.; Nation, J.L. Vegetation indices as indicators of damage by the sunn pest (Hemiptera: Scutelleridae) to field grown wheat. *Afr. J. Biotech.* **2008**, *7*, 173–180.
52. Ashourloo, D.; Mobasheri, M.R.; Huete, A. Developing two spectral disease indices for detection of wheat leaf rust (*Pucciniatriticina*). *Remote Sens.* **2014**, *6*, 4723–4740. [CrossRef]
53. Beltrán, N.H.; Duarte-Mermoud, M.A.; Salah, S.A.; Bustos, M.A.; Peña-Neira, A.I.; Loyola, E.A.; Jalocha, J.W. Feature selection algorithms using Chilean wine chromatograms as examples. *J. Food Eng.* **2005**, *67*, 483–490. [CrossRef]
54. Guyon, I.; Elisseeff, A. An introduction to variable and feature selection. *J. Mach. Learn. Res.* **2003**, *3*, 1157–1182.
55. Schuize, F.H.; Wolf, H.; Jansen, H.; Vander, V.P. Applications of artificial neural networks in integrated water management: Fiction or future? *Water Sci. Technol.* **2005**, *52*, 21–31. [CrossRef]
56. EIMasry, G.; Sun, D.W.; Allen, P. Near-infrared hyperspectral imaging for predicting colour, pH and tenderness of fresh beef. *J. Food Eng.* **2012**, *110*, 127–140. [CrossRef]
57. Strobl, C.; Boulesteix, A.-L.; Kneib, T.; Augustin, T.; Zeileis, A. Conditional variable importance for random forests. *BMC Bioinform.* **2008**, *9*, 307. [CrossRef] [PubMed]
58. Glorfeld, L.W. A methodology for simplification and interpretation of backpropagation-based neural network models. *Expert Syst. Appl.* **1996**, *10*, 37–54. [CrossRef]
59. Melis, G.; Dyer, C.; Blunsom, P. On the state of the art of evaluation in neural language models. *arXiv* **2017**, arXiv:1707.05589.
60. Bergstra, J.; Yamins, D.; Cox, D. Making a science of model search: Hyperparameter optimization in hundreds of dimensions for vision architectures. *ICML* **2013**, *2013*, 115–123.
61. Wu, J.; Chen, X.-Y.; Zhang, H.; Xiong, L.-D.; Lei, H.; Deng, S.-H. Hyperparameter optimization for machine learning models based on Bayesian optimization. *J. Electron. Sci. Technol.* **2019**, *17*, 26–40.

62. Doorenbos, J.; Kassam, A. *Yield Response to Water*; Irrigation and Drainage Paper No. 33; FAO: Rome, Italy, 1986.
63. Vermeiren, L.; Jopling, G.A. *Localized Irrigation*; Irrigation and Drainage Paper No. 36; FAO: Rome, Italy, 1984.
64. James, L.G. *Principles of Farm Irrigation System Design*; John Wiley and Sons, Inc.: Hoboken, NY, USA, 1988.
65. Ismail, S.M. *Design and Management of Field Irrigation System*, 1st ed.; Monshaet El-Maaref: Alexandria, Egypt, 2002; p. 367. (In Arabic)
66. Elsayed, S.; El-Gozayer, K.; Allam, A.; Schmidhalter, U. Passive reflectance sensing using regression and multivariate analysis to estimate biochemical parameters of different fruits kinds. *Sci. Hortic.* **2019**, *243*, 21–33. [CrossRef]
67. Gutierrez, M.; Reynolds, M.P.; Raun, W.R.; Stone, M.L.; Klatt, A.R. Spectral water indices for assessing yield in elite bread wheat genotypes in well irrigated, water stressed, and high temperature conditions. *Crop Sci.* **2010**, *50*, 197–214. [CrossRef]
68. Nagy, A.; Riczu, P.; Tamás, J. Spectral evaluation of apple fruit ripening and pigment content alteration. *Sci. Hortic.* **2016**, *201*, 256–264. [CrossRef]
69. Prasad, B.; Carver, B.F.; Stone, M.L.; Babar, M.A.; Raun, W.R.; Klatt, A.R. Potential use of spectral reflectance indices as a selection tool for grain yield in winter wheat under Great Plains conditions. *Crop Sci.* **2007**, *47*, 1426–1440. [CrossRef]
70. Babar, M.A.; Reynolds, M.P.; Van Ginkel, M.; Klatt, A.R.; Raun, W.R.; Stone, M.L. Spectral reflectance indices as a potential indirect selection criteria for wheat yield under irrigation. *Crop Sci.* **2006**, *46*, 578–588. [CrossRef]
71. Elsayed, S.; Darwish, W. Hyperspectral remote sensing to assess the water status, biomass, and yield of maize cultivars under salinity and water stress. *Bragantia* **2017**, *76*, 62–72. [CrossRef]
72. Han, J.; Kamber, M. *Data Mining: Concepts and Techniques*; Morgan Kaufmann: San Francisco, CA, USA, 2001.
73. Zhu, J.; Huang, Z.H.; Sun, H.; Wang, G.X. Mapping forest ecosystem biomass density for Xiangjiang river basin by combining plot and remote sensing data and comparing spatial extrapolation methods. *Remote Sens.* **2017**, *9*, 241. [CrossRef]
74. Malone, B.P.; Styc, Q.; Minasny, B.; McBratney, A.B. Digital soil mapping of soil carbon at the farm scale: A spatial downscaling approach in consideration of measured and uncertain data. *Geoderma.* **2017**, *290*, 91–99. [CrossRef]
75. Saggi, M.K.; Jain, S. Reference evapotranspiration estimation and modeling of the Punjab Northern India using deep learning. *Comput. Electron. Agric.* **2019**, *156*, 387–398. [CrossRef]
76. Marschner, P. *Marschner's Mineral Nutrition of Higher Plant*, 3rd ed.; Academic Press: London, UK, 2012; pp. 178–189.
77. Jin, S.H.; Huang, J.Q.; Li, X.Q.; Zheng, B.S.; Wu, J.S.; Wang, Z.J.; Liu, G.H.; Chen, M. Effects of potassium supply on limitation of photosynthesis by mesophyll diffusion conductance in Carya cathayensis. *Tree Physiol.* **2011**, *31*, 1142–1151. [CrossRef]
78. Tomemori, H.; Hamamura, K.; Tanabe, K. Interactive effects of sodium and potassium on the growth and photosynthesis of spinach and komatsuna. *Plant Prod. Sci.* **2022**, *5*, 281–285. [CrossRef]
79. Topcu, S.; Kirda, C.; Dasgan, Y.; Kaman, H.; Cetin, M.; Yazici, A.; Bacon, M.A. Yield response and N-fertilizer recovery of tomato grown under deficit irrigation. *Eur. J. Agron.* **2007**, *26*, 64–70. [CrossRef]
80. Anjum, S.A.; Wang, L.; Farooq, M.; Xue, L.; Ali, S. Fulvic acid application improves the maize performance under well-watered and drought conditions. *J. Agron. Crop Sci.* **2011**, *197*, 409–417. [CrossRef]
81. Mafakheri, A.; Siosemardeh, A.; Bahramnejad, B.; Struik, P.C.; Sohrabi, Y. Effect of drought stress on yield, proline and chlorophyll contents in three chickpea cultivars. *Austlian J. Crop Sci.* **2010**, *8*, 580–585.
82. El-Hendawy, S.E.; Alotaibi, M.; Al-Suhaibani, N.; Al-Gaadi, K.; Hassan, W.; Dewir, Y.H.; Emam, M.A.E.-G.; Elsayed, S.; Schmidhalter, U. Comparative performance of spectral reflectance indices and multivariate modeling for assessing agronomic parameters in advanced spring wheat lines under two contrasting irrigation regimes. *Front. Plant Sci.* **2019**, *10*, 1537. [CrossRef] [PubMed]
83. Ranjan, R.; Sahoo, R.; Chopra, U.; Pramanik, M.; Singh, A.; Pradhan, S. Assessment of water status in wheat (*Triticum aestivum* L.) using ground based hyperspectral reflectance. *Proc. Natl. Acad. Sci. USA* **2015**, *87*, 377–388. [CrossRef]
84. Garriga, M.; Romero-Bravo, S.; Estrada, F.; Méndez-Espinoza, A.M.; González-Martínez, L.; Matus, I.A.; Castillo, D.; Lobos, G.A.; Del Pozo, A. Estimating carbon isotope discrimination and grain yield of bread wheat grown under water-limited and full irrigation conditions by hyperspectral canopy reflectance and multilinear regression analysis. *Int. J. Remote Sens.* **2021**, *42*, 2848–2871. [CrossRef]
85. Zhang, L.; Zhou, Z.; Zhang, G.; Meng, Y.; Chen, B.; Wang, Y. Monitoring the leaf water content and specific leaf weight of cotton (*Gossypium hirsutum* L.) in saline soil using leaf spectral reflectance. *Eur. J. Agron.* **2012**, *41*, 103–117. [CrossRef]
86. Zhang, F.; Zhou, G. Estimation of vegetation water content using hyperspectral vegetation indices: A comparison of crop water indicators in response to water stress treatments for summer maize. *BMC Ecol.* **2019**, *19*, 18. [CrossRef]
87. Kawamura, K.; Mackay, A.D.; Tuohy, M.P.; Betteridge, K.; Sanches, I.D.; Inoue, Y. Potential for spectral indices to remotely sense phosphorus and potassium content of legume-based pasture as a means of assessing soil phosphorus and potassium fertility status. *Int. J. Remote Sens.* **2011**, *32*, 103–124. [CrossRef]
88. Lu, J.; Eitel, J.U.H.; Engels, M.; Zhu, J.; Ma, Y.; Liao, F.; Zheng, H.; Wang, X.; Yao, X.; Cheng, T.; et al. Improving Unmanned Aerial Vehicle (UAV) Remote sensing of rice plant potassium accumulation by fusing spectral and textural information. *Int. J. Appl. Earth Obs. Geoinf.* **2021**, *104*, 102592. [CrossRef]
89. Pimstein, A.; Karnieli, A.; Bansal, S.K.; Bonfil, D.J. Exploring remotely sensed technologies for monitoring wheat potassium and phosphorus using field spectroscopy. *Field Crops Res.* **2011**, *121*, 125–135. [CrossRef]
90. Ustin, S.L.; Gamon, J.A. Remote sensing of plant functional types. *New Phytol.* **2010**, *186*, 795–816. [CrossRef] [PubMed]

91. El-Hendawy, S.; Elsayed, S.; Al-Suhaibani, N.; Alotaibi, M.; Tahir, M.U.; Mubushar, M.; Attia, A.; Hassan, W.M. Use of hyperspectral reflectance sensing for assessing growth and chlorophyll content of spring wheat grown under simulated saline field conditions. *Plants* **2021**, *10*, 101. [CrossRef] [PubMed]
92. Elsherbiny, O.; Zhou, L.; Feng, L.; Qiu, Z. Integration of visible and thermal imagery with an artificial neural network approach for robust forecasting of canopy water content in rice. *Remote Sens.* **2021**, *13*, 1785. [CrossRef]
93. Elsherbiny, O.; Fan, Y.; Zhou, L.; Qiu, Z. Fusion of feature selection methods and regression algorithms for predicting the canopy water content of rice based on hyperspectral data. *Agriculture* **2021**, *11*, 51. [CrossRef]